HHS Public Access

Author manuscript

Curr Biol. Author manuscript; available in PMC 2023 October 24.

Published in final edited form as:

Curr Biol. 2022 October 24; 32(20): 4538–4546.e5. doi:10.1016/j.cub.2022.09.005.

Retinoid therapy restores eye-specific cortical responses in adult mice with retinal degeneration

Carey Y. L. Huh[1], **Henri Leinonen**[2,3], **Taylor Nakayama**[1], **Julia R. Tomasello**[1], **Jianye Zhang**[2], **Jack Zeitoun**[1], **John P. Peach**[4], **Maximilian Halabi**[2,5], **Jianying Z. Kiser**[2], **Krzysztof Palczewski**[2,5,6], **Philip D. Kiser**[2,5,7,8], **Sunil P. Gandhi**[1,9,*]

[1]Department of Neurobiology and Behavior, University of California, Irvine; Irvine, CA, 92697, USA.

[2]Gavin Herbert Eye Institute, Department of Ophthalmology, Center for Translational Vision Research, University of California, Irvine; Irvine, CA, 92697, USA.

[3]School of Pharmacy, Faculty of Health Sciences, University of Eastern Finland; Kuopio, 70211, Finland.

[4]Whiting School of Engineering, Johns Hopkins University; Baltimore, MD, 21218, USA.

[5]Department of Physiology & Biophysics, University of California, Irvine; Irvine, CA, 92697, USA.

[6]Department of Chemistry, University of California, Irvine; Irvine, CA, 92697, USA.

[7]Research Service, VA Long Beach Healthcare System; Long Beach, CA, 90822, USA.

[8]Department of Clinical Pharmacy Practice, University of California, Irvine; Irvine, CA, 92697, USA.

[9]Center for the Neurobiology of Learning and Memory, University of California, Irvine; Irvine, CA, 92697, USA.

Summary

Despite the recent emergence of multiple cellular and molecular strategies to restore vision in retinal disorders, it remains unclear to what extent central visual circuits can recover when retinal

*Corresponding author and Lead contact. spgandhi@uci.edu, Twitter handle: @drsunilgandhi.

Author contributions

Conceptualization: CYLH, PDK, KP, SPG
Methodology: CYLH, PDK, J. Zhang, J. Zeitoun, JPP, HL, KP, SPG
Investigation: CYLH, PDK, HL, TN, JRT, JZK
Visualization: CYLH, PDK, HL
Funding acquisition: PDK, KP, SPG
Project administration: PDK, KP, SPG
Supervision: PDK, KP, SPG
Writing – CYLH, PDK
Writing – review & editing: CYLH, HL, PDK, TN, JRT, KP, SPG

Declaration of interests

S.P.G. is co-founder and Chief Scientific Advisor of Translucence Biosystems, Inc. and co-founder and Chief Technology Officer of NovoGlia, Inc. K.P. is the Chief Scientific Officer of Polgenix Inc. and consultant of Prime Medicine, and Editas Medicine.

defects are corrected in adulthood. We addressed this question in an *Lrat*$^{-/-}$ mouse model of Leber congenital amaurosis (LCA) in which retinal light sensitivity and optomotor responses are partially restored by 9-*cis*-retinyl acetate administration in adulthood. Following treatment, two-photon calcium imaging revealed increases in the number and response amplitude of visually responsive neurons in the primary visual cortex (V1). In particular, retinoid treatment enhanced responses from the ipsilateral eye, restoring the normal balance of eye-specific responses in V1. Additionally, the treatment rescued the modulation of cortical responses by arousal. These findings illustrate the significant plasticity of the adult central visual system and underscore the therapeutic potential of retinoid administration for adults with retinal diseases.

eTOC Blurb

Huh *et al.* report that a mouse model of retinal degeneration can undergo a significant restoration of vision when treated with retinoid therapy. Several visual properties in V1 are fully restored even when the therapy is started in adulthood, showcasing the potential of retinoid compounds as promising therapeutics for treating retinal diseases.

Graphical Abstract

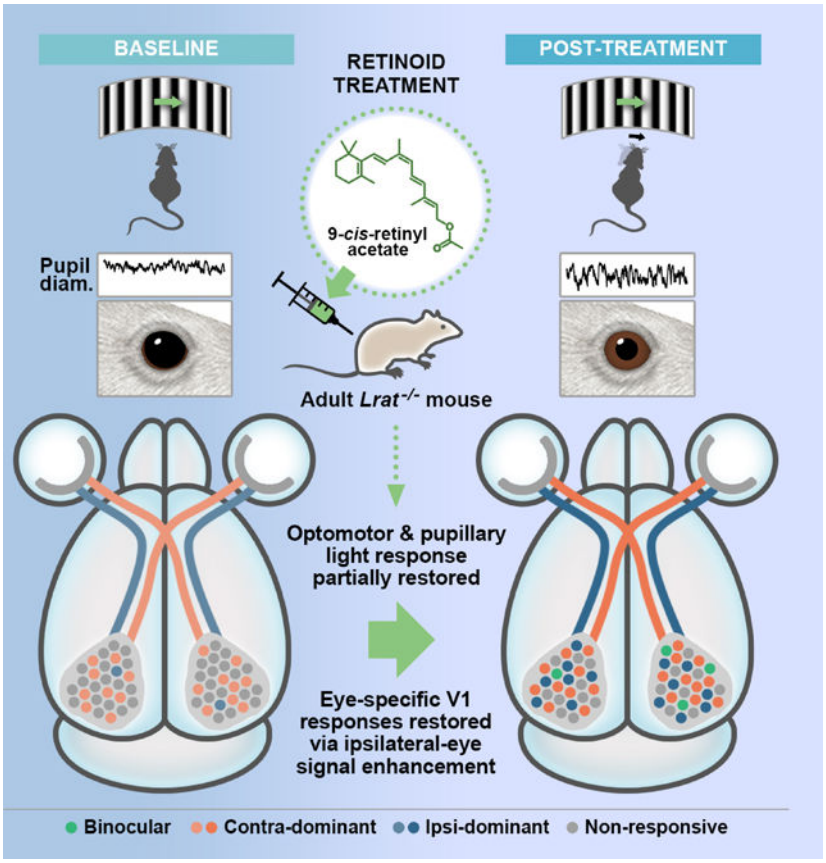

Results and Discussion

Effective treatment for childhood blinding diseases involving retinal dysfunction remains one of the major unmet needs in medicine[1]. Over the last two decades, numerous strategies have emerged, including gene replacement therapy[2], gene editing approaches[3], optogenetics[4], retinal electrical implants[5], iPSC-derived retinal cell replacements[6], and pharmacological agents[7–9]. These approaches can restore light-sensing ability at the retinal level and lead to improvements in visual perception in patients to varying extents. Studies of synthetic retinoid treatment in patients with *RPE65* or *LRAT* mutations have led to improvements in visual field area and visual cortex activation, as seen on fMRI scans[10–12]. A separate study using intravitreally-administered synthetic retinoid to treat RPE65-mutant dogs found that electroretinogram (ERG) recordings recovered a normal shape and response threshold following treatment, although the duration of this effect was limited to ten weeks. The treatment also improved vision-dependent behavioral tests at low light intensities[13]. Clinical trials of gene therapy for recessive RPE65-associated retinopathies have also demonstrated behavioral and visual field area improvements and increases in visual cortex fMRI signals in treated patients and dogs[2,14–16]. Indeed, measures of visual cortex activity may provide an objective way to assess long-term treatment efficacy[17]. Although some progress has been made[3,18,19], it still remains unclear the extent to which adult visual circuits can be restored to a fully functional state at the level of the visual cortex upon correction of the retinal defect.

It is widely appreciated that visual impairments in early critical periods of postnatal development can lead to lifelong deficits in central visual function, even when the initial abnormality is corrected[20]. Recent studies have revealed exceptions to this critical period restriction[21]. How the critical period applies to visual circuit remodeling in response to restoration of retinal function has not been defined. This question is crucial as its answer would inform the optimal timing of visual restoration efforts.

We employed an established model of a childhood blinding disease, the lecithin:retinol acyltransferase knockout (*Lrat*$^{-/-}$) mouse to determine the extent of recovery of the central visual circuit following acute rescue of retinal light sensitivity. The *Lrat*$^{-/-}$ mouse has a metabolic blockade in the visual cycle pathway that produces the visual chromophore, 11-*cis*-retinal, necessary for the formation of photoreceptor visual pigments, thus recapitulating the primary pathology associated with Leber congenital amaurosis (LCA) type 14[22] (Figure 1A). This blockade can be circumvented pharmacologically by administration of a retinoid, 9-*cis*-retinyl acetate (9-*cis*-R-Ac). 9-*cis*-R-Ac, a 9-*cis*-retinal prodrug, is currently under clinical investigation as a visual chromophore substitute[8,10,12]. We confirmed that intraperitoneal administration of 9-*cis*-R-Ac (40 mg/kg in DMSO) to *Lrat*$^{-/-}$ mice for seven consecutive days led to substantial 9-*cis*-retinal accumulation in the eye (Figure S1A–C) and produced a rapid and prolonged improvement in light-induced ERG activity and optomotor reflexes (OMR) as compared to vehicle (DMSO) control (Figure 1B–H). Prior studies have shown that cone photoreceptors completely degenerate in *Lrat*$^{-/-}$ mice by postnatal day 42[23,24]. Consistently, we observed no M-cone opsin immunostaining in the *Lrat*$^{-/-}$ mice used for our experiments, irrespective of retinoid treatment (Figure S2), which strongly indicated that the ERG and OMR improvements arose from restoration of

rod photoreceptor function. We next employed widefield intrinsic signal optical imaging and two-photon calcium imaging to measure changes in primary visual cortex (V1) neuronal activity following retinoid treatment.

We first investigated the effect of 9-*cis*-R-Ac treatment on V1 activation in adult *Lrat*$^{-/-}$ mice using widefield intrinsic signal optical imaging (ISOI) which provides a bulk measure of visual activity (Figure 2A). Prior to treatment at baseline, *Lrat*$^{-/-}$ mice exhibited poor visual activation of V1 compared to wild-type mice (Figure 2B). *Lrat*$^{-/-}$ mice were administered either retinoid or vehicle daily for seven days (Figure 2C). We found that 9-*cis*-R-Ac treatment led to a significant increase in the amplitude of V1 activation (median of 28% increase when using stimuli with max. luminance of 33 cd/m^2; Figure 2D–G). The increased amplitude in retinoid-treated mice was sustained for at least 9 days post-treatment and provided therapeutic effects at 27 days post-treatment compared to the vehicle (Figure 2E–G). Behavioral (OMR) improvements were sustained for at least 19–20 days post-treatment (Figure 1F–H). By contrast, vehicle-treated mice exhibited a progressive decrease in response amplitude over time (Figure 2D–E, G). To investigate the nature of this progressive decline, we evaluated V1 activation in repeated ISOI imaging recordings in age-matched wild-type mice. Wild-type mice displayed a similar level of reduction in visual response amplitude with time, as we observed with vehicle-treated *Lrat*$^{-/-}$ mice (Figure 2E–G). We speculate that these changes reflect an expected level of degradation in signal due in part to visual adaptation to repeated stimuli under awake recording conditions and likely do not indicate further decline of visual function in *Lrat*$^{-/-}$ mice over a relatively short period of time.

Since 9-*cis*-R-Ac partially restores photoreceptor function in *Lrat*$^{-/-}$ mice[25] (Figure 1C–E), the effect on visually evoked activity in V1 as observed using ISOI may be explained by improved retinal signals leading to: 1) activation of a greater number of V1 neurons, 2) increased response amplitude per neuron, or 3) both. To examine these possibilities, we measured neuronal activity in V1 at cellular resolution using two-photon calcium imaging. Adult *Lrat*$^{-/-}$ mice were injected with a syn-GCaMP6s virus into the binocular zone of V1, implanted with a cranial window, and treated with seven days of 9-*cis*-R-Ac. Typically the same sets of V1 neurons were recorded at baseline, within one day following the end of treatment, and nine days post-treatment (Figure 3A). Neuronal activity was measured while mice viewed stimuli through both eyes, the contralateral (“contra”) eye, or the ipsilateral (“ipsi”) eye, relative to the recorded hemisphere (Figure 3B).

Two-photon calcium imaging revealed that 9-*cis*-R-Ac treatment led to a significant increase in the response amplitude of individual V1 neurons (mean of two-fold increase when using stimuli with max. luminance of 33 cd/m^2) and that this effect reversed during the post-treatment period (Figure 3C–D). The number of neurons visually responsive to both- and contra-eye stimulation doubled after treatment, an effect that was largely reversed during the post period (Figure 3E). Strikingly, the number of neurons activated by ipsi-eye stimulation increased by nearly five-fold after treatment, an increase that was sustained during the post period (Figure 3E). We confirmed using ISOI that the effect of treatment on V1 activation through the ipsilateral eye was observed at both low and high visual luminance levels (max.

luminance of 33 and 330 cd/m^2; Figure S3), indicating that even at high luminance levels, the cortical response to the ipsilateral-eye stimulation is enhanced by the treatment.

Two-photon calcium imaging further revealed that V1 neurons displayed broader orientation tuning, preference for higher spatial frequencies (SF), and larger SF bandwidth following treatment (Figure S4). The higher SF preference and broader SF tuning effects were transient, whereas the broader orientation tuning effect remained at post (Figure S4). These results indicate that *Lrat*$^{-/-}$ V1 increased in terms of response strength, number of activated neurons and stimulus bandwidth. While the enhancement of the contralateral-eye signal was transient, the ipsilateral-eye signal underwent a particularly prominent and long-lasting improvement.

Given that 9-*cis*-R-Ac led to differential effects on *Lrat*$^{-/-}$ V1 responses depending on which eye was stimulated, we examined the effects on V1 neurons' ocular dominance properties. Ocular dominance index (ODI) values near 1 indicate contra-eye dominance, values near −1 indicate ipsi-eye dominance, and values near zero indicate significant responses to both eyes (binocular). At baseline, V1 neurons in *Lrat*$^{-/-}$ mice displayed severely abnormal ODI with mostly contra-dominant cells (Figure 3F–H). Immediately after retinoid treatment, ODI distributions shifted such that greater proportions of neurons displayed ipsi-dominant or binocular responses (Figure 3F–H). However, ODI distributions in *Lrat*$^{-/-}$ mice did not fully shift to normal until the post period, becoming indistinguishable from those found in wild-type mice (Figure 2F–H), indicating that binocular circuits in *Lrat*$^{-/-}$ mice take time to restore to normal following treatment.

One explanation for the increased ipsi-dominant population after treatment of the *Lrat*$^{-/-}$ mice is that newly ipsi-dominant neurons arise from a pool previously non-responsive to visual stimuli. Or, the newly ipsi-dominant neurons are originally contra-dominant or binocular neurons, and switch their OD properties after treatment. To distinguish between these mechanisms, we tracked the activity of the same neurons over time. We designated neurons as "ipsi-destined", "contra-destined", or "binocular-destined" based on their post-period responses, and compared them with their prior OD identity at baseline and after treatment. While the majority of ipsi-destined neurons originated from a previously non-responsive pool of neurons (44/68 or 65%; Figure 3J), we found an unexpectedly large proportion of ipsi-destined neurons that were previously contra-dominant (18/68 or 26%; Figure 3I,J). This form of OD plasticity - monocular neurons switching OD to the other eye - is surprising as it rarely occurs during juvenile development[26]. The small remainder of the ipsi-destined population were either already ipsi-dominant neurons (4/68 or 6%) or neurons that switched OD status between baseline and treatment ("other", 2/68 or 3%; Figure 3J).

Although some visual properties in V1 were restored by 9-*cis*-R-Ac treatment in adult *Lrat*$^{-/-}$ mice, it is unclear whether the recovery extends to functions involving multiple visual pathways. Arousal-mediated modulation of the visual system involves the coordination of multiple circuits and undergoes prolonged periods of development[27,28]. To investigate arousal-mediated V1 modulation, we performed pupil tracking during two-photon calcium imaging of V1 neurons (Figure 4A). At baseline, *Lrat*$^{-/-}$ mice displayed large pupils with minimal size modulation compared to those found in wild-type mice,

suggesting that their pupils are constantly enlarged with little arousal-mediated modulation (Figure 4B). Following retinoid treatment, mean pupil size was reduced but remained larger than wild-type mice under similar light conditions (Figure 4B,C). The amplitude of pupil size modulation was abnormally low in *Lrat*$^{-/-}$ mice and following treatment, pupil size modulation became larger and was indistinguishable from wild-type values by the end of the post treatment period (Figure 4D). However, we note that pupil size modulation may have been low at baseline in *Lrat*$^{-/-}$ mice partially due to ceiling effects of their abnormally large pupil sizes.

Within normal mice, V1 neuronal activity is tightly correlated with pupil size fluctuations[27,29]. Accordingly, we found that the population calcium trace (average of individual traces) closely recapitulated the minute-to-minute pupil size fluctuations in wild-type mice (Figure 4E, the rightmost panel, top 2 traces). In wild-type mice, we found high cross-correlation between the pupil diameter trace and individual neurons' calcium traces, with neural signals leading pupil fluctuations (negative pupil-neural lag; 4th panel in Figure 4F). By contrast, *Lrat*$^{-/-}$ mice displayed little correlation between pupil and neural signals before treatment (Figure 4E–G, Baseline). Following retinoid treatment, pupil and neural traces for *Lrat*$^{-/-}$ mice became more correlated such that correlation values became similar to wild-type values (Figure 4G). Cross-correlation values also became higher in negative pupil-neural lag windows compared to positive lag windows, indicating that neural signals led pupil traces in treated *Lrat*$^{-/-}$ mice (Figure 4F).

The extent of central vision recovery observed in our study is notable, given that *Lrat*$^{-/-}$ mice have dramatically reduced photoreceptor function[25], virtually no cone outer segments and only ~30% of the rod outer segments remaining by one month of age[23]. We found that at baseline, adult *Lrat*$^{-/-}$ mice display poor activation of V1 by visual stimuli and ocular dominance distributions in V1 neurons that are abnormally skewed towards contralateral-eye dominance. Following 9-*cis*-R-Ac treatment, some properties such as visual response amplitude were increased immediately after treatment and reversed by post period. We speculate that some of these immediate and short-lasting effects may be due to circuit-wide changes in gain. In particular, the mean response amplitude in *Lrat*$^{-/-}$ mice immediately following treatment was numerically higher compared to responses in wild-type mice (Figure 3D and ISOI results in Figure 2F) although the differences were not statistically significant. In addition, *Lrat*$^{-/-}$ V1 neurons' preferred spatial frequency and spatial frequency tuning bandwidth after treatment were higher and broader, respectively, compared to wild-type values (Figure S4B,C). We speculate that these transient overshoots may in part be due to the dark exposure during the treatment period shifting the excitatory-inhibitory balance in favor of excitation in cortical circuits, as previously shown in the visual cortex[30]. In *Lrat*$^{-/-}$ mice, inhibitory circuits may be especially underdeveloped because of the prolonged lack of retinal signals. Immediately following treatment, stronger visual signals may reach V1 circuits due to the partially restored photoreceptor function, and inhibitory circuits may not be strong enough yet to counteract the excitation. The reduced inhibitory tone may also explain the broadening of orientation selectivity seen post-treatment (Figure S4A). After some time (by post period), the excitatory-inhibitory balance may become partially re-established. Whether dark exposure during the treatment period plays a significant role in the over-activation of V1 during treatment remains to

be determined. Intriguingly, in a clinical trial of 9-*cis*-R-Ac, some LCA patients reported photophobia[10] which may be consistent with V1 over-activation.

Visual function changes that take longer to manifest and are longer-lasting (*e.g.*, increases in the number of ipsilateral-eye responsive neurons and changes in ocular dominance distribution) may reflect new synapses being formed. With stronger input from retinae, new synapses may be added or existing synapses recruited to relay signals from the ipsilateral eye. Interestingly, we found that the majority of the newly ipsi-dominant neurons arose from previously non-responsive or contra-dominant neurons, which suggest not only a *de novo* cortical activity but a shift in visual tuning properties. The locus of these changes in the visual pathway (in thalamus[31] or V1) and underlying mechanisms remain to be investigated in future studies. It also remains to be determined the extent to which the increase in light sensitivity in the retina after the treatment contributes to recruitment of a greater number of V1 neurons. Our immunohistochemistry results indicate that all visual responses in *Lrat*$^{-/-}$ mice at the adult age we examined, even in those that were treated, originate from rod photoreceptors. It remains to be explored whether a similar extent of central circuit restoration is possible in other models of retinal degeneration.

Our ISOI results show a sustained increase in V1 response that lasts until nine days post treatment, but two-photon calcium imaging results show a transient increase that is not sustained until 9 d post treatment. These differences may reflect the nature of the two signals. ISOI measures oxygenated blood in a large volume of tissue resulting from a combination of neuronal firing and neuropil activity (input from other cortical layers and brain areas). In contrast, two-photon calcium imaging reports activity at the level of single neurons in the specific area and layers that were imaged (V1 L2/3 in our case). It may be that activity in circuits other than V1 L2/3 are restored in a sustained manner (*e.g.,* deeper-layer neurons in V1, projection neurons in higher visual areas) whereas V1 L2/3 neurons show a transient increase, and ISOI amplitude may reflect increased inputs from these sources.

In our study, measures of subcortical visual functions were only partially rescued, yet many of the higher-level (V1) visual functions indicated restoration to normal levels. Previous studies that administered retinoid therapies to LCA patients reported that many experienced long-lasting improvements in visual acuity and visual field area[10,12]. In these and other studies[10,32,33], no changes in ERG measurements were observed despite significant subjective improvements in visual perception. Likewise in our study, improvements at the retina and those reflecting subcortical changes (*e.g.,* ERG, pupil size, and OMR responses) indicated partial recovery while many properties in the visual cortex were fully restored to normal levels (visual response amplitude, ocular dominance and pupil-neural correlation). Together, these findings suggest that therapeutic interventions can lead to a much greater extent of central vision recovery than expected from retinal readings alone.

In summary, our findings indicate that a mouse model of retinal degeneration can undergo a significant restoration of vision when treated with retinoid replacement therapy, even in adulthood. V1 visual responses, both in terms of the number of visually responsive neurons and the strength of visual response per neuron, were strongly enhanced by the treatment.

Ipsilateral eye visual processing, arousal-mediated modulation of neuronal activity in V1, and optomotor behavior showed marked improvements that lasted well beyond the end of the treatment. Although our finding of restored ocular dominance distribution suggests at least a partial restoration of binocular circuits, future studies using behavioral assays will be needed to fully assess whether binocular (depth) vision is restored by retinoid treatment in adulthood. Our results reveal an unexpected and promising plasticity of the visual circuit, suggesting that therapeutic strategies for childhood blinding diseases can be highly effective even if intervention is started in adulthood. Despite demonstrated efficacy, ease of oral administration, and excellent safety profile, retinoid therapies have remained relatively under-explored until recent years[34]. Our findings showcase the potential of retinoid compounds as promising therapeutics for treating numerous retinal diseases involving defects in the visual cycle.

STAR Methods

RESOURCE AVAILABILITY

Lead contact—Further information and requests for resources and reagents should be directed to and will be fulfilled by the lead contact, Sunil P. Gandhi (spgandhi@uci.edu).

Materials availability—This study did not generate new unique reagents.

Data and code availability

- Data have been deposited at GitHub and are publicly available as of the date of publication. DOIs are listed in the key resources table.
- All original code has been deposited at GitHub and is publicly available as of the date of publication. DOIs are listed in the key resources table.
- Any additional information required to reanalyze the data reported in this paper is available from the lead contact upon request.

EXPERIMENTAL MODEL AND SUBJECT DETAILS

Animals—Animal procedures were approved by the Institutional Animal Care and Use Committees at the VA Long Beach Healthcare System and the University of California Irvine. All experimental protocols were conducted in accordance with the NIH Guide for the Care and Use of Laboratory Animals, the recommendations of the American Veterinary Medical Association Panel on Euthanasia, and the Association for Research in Vision and Ophthalmology Statement for the Use of Animals in Ophthalmic and Visual Research.

For all experiments, both sexes of mice were used. All mice were housed in a standard 12/12-h light/dark cycle environment or in a devoted dark room when being used for experiments. Animals were fed standard soy protein-free rodent chow diet (Envigo Teklad 2020X), provided water *ad libitum*, and housed in plastic cages with standard corncob rodent bedding and 6 g nestlets (Ancare).

Pigmented *Lrat*$^{-/-}$ mice[22] (RRID:IMSR_JAX:018866) or wild-type C57BL/6 mice (RRID:IMSR_CRL:027; RRID:IMSR_JAX:000664) were used for experiments. For

experiments in Figure 1, *Lrat*$^{-/-}$ and wild-type mice at ages of postnatal days (P) 70 – 77 were used. For V1 imaging experiments, *Lrat*$^{-/-}$ and wild-type mice were P60–78 at the time of baseline imaging sessions (mean age: P69).

METHOD DETAILS

Retinoid synthesis and treatment—9-*cis*-retinyl acetate (9-*cis*-R-Ac) was prepared as described previously[35]. Briefly, 0.1 mg of bis(benzonitrile)palladium chloride was added to a solution of all-*trans*-retinyl acetate (100 g) in hexanes (200 ml) and trimethylamine (55 μl), and the mixture was stirred overnight in the dark at 65 °C. The resulting solution was cooled to −80 °C overnight and filtered by suction using a precooled filter. Sixty microliters of the filtrate were injected into an Agilent 1100 HPLC system (Santa Clara, CA) and chromatographed on a silica Luna column (10 μ, 100 Å, 250 × 21.2 mm, Phenomenex, Torrance, CA) to afford 10 mg of 9-*cis*-R-Ac. The injection and separation were repeated until sufficient amounts of pure 9-*cis*-R-Ac were obtained. Purified 9-*cis*-R-Ac was dried *in vacuo* and then reconstituted in DMSO for administration to mice.

Prior to the first injection, *Lrat*$^{-/-}$ mice were individually housed, weighed, and dark adapted for >12 hr. Under dim red light, *Lrat*$^{-/-}$ mice were administered 9-*cis*-R-Ac at a dose of 40 mg/kg in DMSO, or DMSO only (vehicle control), *via* intraperitoneal injection once daily for seven consecutive days. This dosage was well tolerated by adult (≥P60) mice.

GCaMP6s virus delivery and cranial window implantation—For two-photon calcium imaging, mice (age: P39–57, mean: P43) were injected with viral vectors to express GCaMP6s (pAAV.Syn.GCaMP6s.WPRE.SV40(AAV1); Addgene 100843-AAV1) in neurons in the binocular zone of the primary visual cortex (V1). Mice were placed in a stereotaxic frame under isoflurane anesthesia (2% for induction, <1% for maintenance). Body temperature was maintained at ~37 °C by a feedback-controlled heat pad and eyes were covered with ophthalmic ointment. Mice were injected with carprofen (5 mg/kg, s.c.) and lactated Ringer's solution for analgesia and hydration. The scalp was shaved and the incision site was prepared with ethanol, iodine and topical lidocaine (2%). With the head secured using earbars, the scalp was retracted and a small burr hole was made at the injection site using a pneumatic drill. Coordinates used for targeting the binocular zone of V1 were 2.8 mm lateral from the midline, 1.0 mm anterior from the back suture. Viral vectors diluted to the final titer of $1 \times 10^{11} – 10^{12}$ GC/ml were loaded into a glass pipette and injected into V1 in the right hemisphere. Injections were made at two depths: 0.4 and 0.35 mm deep from the brain surface (200 nl per depth, total volume: 400 nl, rate: 20 nl/min). The skull and injection site were kept moist with saline during the injection. Following surgery, mice were placed on a heat pad to recover and monitored for post-operative health.

For two-photon calcium imaging and widefield intrinsic signal imaging, a headplate was attached and a cranial window was installed. Two hr prior to the surgery, mice (age: P52–71, mean: P59) were injected with dexamethasone (4.8 mg/kg, i.m.). After administration of carprofen (5 mg/kg, s.c.), atropine (0.15 mg/kg, s.c.) and lactated Ringer's solution, mice were anesthetized with isoflurane, placed in a stereotaxic frame and the head secured. After incision site preparation, the skull was exposed and approximate binocular V1 coordinates

were marked. A layer of cyanoacrylic glue (3M Vetbond™) was applied to the skull and a custom-printed black headplate was centered over the marked location and fixed to the skull using black dental acrylic (Ortho-Jet, Lang Dental) at an angle parallel to the imaging site. A craniotomy was performed and a No. 1 (4 mm diameter) glass coverslip was placed over the exposed brain and sealed with cyanoacrylic glue and dental acrylic. Mice were placed in a warm cage to recover until mobile and given daily injections of carprofen and lactated Ringer's solution for ≥5 days and monitored for post-operative health.

Widefield intrinsic signal optical imaging (ISOI)—For experiments shown in Figure 2, widefield ISOI was performed in awake animals through the cranial window after ≥6 days of recovery following craniotomy. Mice were habituated on the setup for 0.5 – 1 hr prior to the first imaging session. Mice were placed on a smooth platform and head-fixed, and a full-contrast noise stimulus was shown to the mice that spanned the central 30° of visual field. The stimulus was a band-limited (<0.05 cpd, >2 Hz) binarized spatiotemporal noise movie with a one-dimensional Gaussian spatial mask (30°), generated using custom Python scripts. The contrast-reversing stimulus moved either up or down periodically every 20 sec, presented on a gamma-corrected 24-inch LED monitor (ASUS VG248, 60 Hz refresh rate, 20 cd/m^2 mean luminance, 33 cd/m^2 maximum luminance) at a viewing distance of 25 cm. Widefield images were acquired using a SciMedia THT macroscope (Leica PlanApo 1.0X, 6.5 × 6.5 mm imaging area) with an Andor Zyla sCMOS camera. Using a green (530 nm) LED, the camera view was centered on the cranial window and focused ~600 μm into the brain under the surface vasculature. ISOI signals were acquired with a red (617 nm) LED. Under binocular viewing conditions, the stimulus was presented for 5 min and typically 2 – 3 repeats were run for each direction (up or down).

For experiments shown in Figure S3, widefield ISOI was performed through intact skull under isofluorane anesthesia (2% for induction, <1% for maintenance). Body temperature was maintained at ~37 °C by a feedback-controlled heating pad and eyes were covered with silicone oil to prevent drying. The stimulus presented was the same as for awake recordings, except that two different maximum luminance levels were used: 33 and 330 cd/m^2. Recordings were performed under monocular viewing conditions, alternating between the eyes ipsilateral and contralateral to the recorded hemisphere. Other details of data acquisition were the same as for awake recordings.

Data were analyzed using custom MATLAB (MathWorks) software to output amplitude and phase maps of cortical activation by extracting signals that varied at the frequency of stimulus repetition (0.05 Hz)[36]. Peak amplitude was computed by taking the maximum of the Fourier amplitude map.

Two-photon calcium imaging and pupil imaging—*In vivo* two-photon calcium imaging was performed on awake head-fixed mice sitting on a smooth surface. Mice were habituated on the imaging setup for 0.5 – 1 hr prior to the first imaging day. Typically, the same fields of view in the binocular zone of V1 were recorded over several sessions, for 2 – 3 hr per day. If the sets of neurons from a previous session could not be identified, different fields of view in V1 were recorded. The average time interval between GCaMP6s virus

injection and the first two-photon imaging session was 23 days (age at baseline imaging session: P60–78, mean: P69).

GCaMP6s imaging was performed using a resonant two-photon microscope (Neurolabware), 920 nm excitation laser (Mai Tai HP, Spectra-Physics) and a Nikon 16X (NA = 0.8) water-immersion objective. Typical fields of view were acquired at 4x zoom, covering a rectangular field of view of ~450 μm × 550 μm and image sequences were acquired at 8 Hz (990 lines) at approximately 200 μm below the brain surface, corresponding to cortical layers 2/3. Data acquisition was controlled by Scanbox software (Neurolabware).

Visual stimuli were presented on a gamma-corrected 24-inch LED monitor (Asus VG248, 60 Hz refresh rate, 20 cd/m^2), placed at 25 cm from the mouse's eyes. Stimuli were generated by custom Python software using the PsychoPy 1.9 library. They were spherically corrected, and included full-field drifting sinusoidal gratings (contrast: 99%) of 6 spatial frequencies (SF; 0.03 – 0.96 cpd, spaced logarithmically) and 8 directions (0 – 315°, in 45° steps) at a temporal frequency of 2 Hz, a blank (uniform luminance) stimulus, and a full-field flicker (2 Hz) stimulus. Each trial consisted of a uniform gray screen for 2 sec and a visual stimulus for 2 sec. Eight repeats per stimulus were presented in a random order without replacement. For monocular viewing, stimuli were presented to one eye at a time, either first to the contralateral or ipsilateral eye using an occluder. The order of eye presentation was chosen randomly for each session. For binocular viewing, no occluder was used.

Two-photon calcium movies were motion-corrected and processed for extracting fluorescence traces using custom Python software. Motion leading to translational artifacts was corrected using a Fourier transform approach[37]. Using a summed intensity projection of the motion-corrected movies, we applied morphological criteria to manually identify regions of interest (ROIs) that correspond to neuronal somata. Pixel values within the ROI were averaged to yield the fluorescence trace of the ROI. The fluorescence signal of a ROI at time t was determined[38,39] as follows: $F_{cell}(t) = F_{soma}(t) - (R \cdot F_{neuropil}(t))$. We empirically determined R to be 0.7 by comparing blood-vessel intensity of the GCaMP6s signal to that in the neuropil. The neuropil signal was estimated by averaging values in pixels within ~3 μm radius outside the cell's outline.

To calculate a response amplitude of an ROI to the stimulus ($\Delta F/F_0$), the calcium trace during the stimulation period was normalized to the baseline value (0.5 sec preceding the stimulus). The mean $\Delta F/F_0$ was generated by averaging normalized responses across all the repeats of the stimulus. The mean response amplitude of the ROI during blank stimulus presentation was used to estimate the spontaneous calcium fluctuation. For each SF, the visual responsiveness of an ROI was determined using a one-way ANOVA ($P < 0.01$) across responses for all orientations for that SF against responses for the blank condition. For analysis of visual response properties (with the exception of pupil-neural cross-correlation analysis), we used responsiveness criteria where only ROIs whose responses at the preferred SF (SF that gave the strongest response) reached statistical significance at $P < 0.01$ were examined. Considering only neurons with preferred SF between 0.06 and 0.48 cpd (inclusive), the SF tuning curve was fitted with a Gaussian function, and the bandwidth

was calculated by taking the square root of the width at half the maximum of the fit. For statistical analysis of preferred SF and response amplitude values, log-transformed values were used. Global orientation selectivity index (gOSI) was determined using a method based on circular variance of the cell's response as follows.

$$gOSI = \frac{\sqrt{(\Sigma_i F(\Theta_i)\sin 2\Theta_i)^2 + (\Sigma_i F(\Theta_i)\cos 2\Theta_i)^2}}{\Sigma_i F(\Theta_i)}$$

where $F(\theta_i)$ is the averaged amplitude of a cell's response to a stimulus orientation θ.

Ocular dominance index (ODI) for each ROI was calculated as $(C - I)/(C + I)$, where C is contralateral-eye response amplitude and I is ipsilateral-eye response amplitude; response amplitude is the mean $\Delta F/F_0$ as described above. For ROIs that did not show a significant response for one of the eyes according to the responsiveness criteria described above, response amplitude for that eye was set to zero. Such neurons were deemed functionally monocular and described as contralaterally (contra)-dominant or ipsilaterally (ipsi)-dominant (ODI values of 1 or −1, respectively). We note that other studies typically have not probed spatial frequencies above 0.48 cpd as we have done here and we have found that probing at higher SF's is important because many high-SF responsive V1 cells are monocular[40]. The wild-type ODI distribution we report here is consistent with those from previous studies from our and other groups[31,41,42].

Eye tracking was achieved using IR-compatible GigE cameras (Allied Vision Mako-131B) and illumination by the infrared laser was used for two-photon imaging. Eye tracking movies were acquired simultaneously with two-photon calcium imaging. To identify the pupils, contours were extracted from each movie frame using routines from the Python OpenCV library (version 3.2.0). Accuracy of pupil detection was visually checked and frames with artifacts and/or blinks were removed by an experimenter naive to the purpose of the experiment. For pupil-neural correlation analysis, calcium traces from all ROI's were included, regardless of passing the responsiveness criteria. The mean and standard deviation of pupil diameter were calculated from recordings that were typically 26 min long and acquired at 8 frames/sec. Although eye tracking movies were acquired for both eyes, only one (left) eye recording was used for pupil-neural correlation, as preliminary analysis showed that pupil diameter was essentially indistinguishable between the two eyes. Pupil diameter values were first normalized and values at 5 z-scores away from the mean were excluded. Calcium traces from neural data were first de-trended and normalized. To de-trend, the lm function in the stats package in R was used to fit a linear model to the calcium trace and residuals were computed to obtain de-trended data, where residuals were the difference between the data and fitted values. Cross-correlation values between the pupil diameter trace and individual calcium traces were calculated at different pupil-neural lags, using the ccf function in the stats package in R. The pupil-neural lag is negative when neural signal is leading; it is positive when pupil signal is leading. The maximum cross-correlation value from each cell was used for statistical comparison.

Electroretinography—Electroretinography (ERG) was performed in a dark room using a Diagnosys Celeris rodent ERG device (Diagnosys, Lowell, MA), as described previously[43].

Under dim red light, the dark-adapted mice were anesthetized with ketamine (100 mg/kg, KetaVed; Bioniche Teoranta, Inverin Co., Galway, Ireland) and xylazine (10 mg/mg, Rompun; Bayer, Shawnee Mission, KS) by intraperitoneal injection, and their pupils were dilated with 1% tropicamide (Tropicamide Ophthalmic Solution USP 1%; Akorn, Lake Forest, IL) and thereafter kept moist with 0.3% hypromellose gel (GenTeal; Alcon, Fort Worth, TX). An additional 3 min were allowed in full dark adaptation before recordings were initiated. Light stimulation was produced by an in-house scripted stimulation series in Espion software (version 6; Diagnosys). The eyes were stimulated with a green light-emitting diode (LED) (peak 544 nm, bandwidth 160 nm) using a 11-step ascending flash strength series between 0.0002 and 100 cd·s/m^2. The ERG signal was acquired at 2 kHz and filtered with a low-frequency cutoff at 0.25 Hz and a high-frequency cutoff at 300 Hz. Espion software automatically detected the ERG a-wave (first negative ERG component) and b-wave (first positive ERG component) amplitudes; a-wave amplitude was measured from the signal baseline, whereas b- wave amplitude was measured as the difference between the negative trough (a-wave) and the highest positive peak.

Optomotor reflex test—The optomotor reflexes (OMR) were assessed using a commercial OMR platform (Phenosys qOMR, PhenoSys GmbH, Berlin, Germany) that utilizes automated head tracking and behavior analysis, following protocols described earlier[3]. The OMR arena was dimmed using neutral density filters in front of the stimulus displays. The ambient luminance was measured at ~1 lux, corresponding to roughly twilight light level. Rotating (12° sec^{-1}) vertical sinusoidal grating stimuli at changing contrast levels were presented for 12 min per trial to initially dark-adapted mice. The spatial frequency of the grating was set at 0.1 cycles per degree of the visual angle whereas the pattern contrast (5, 7.5, 10, 12.5, 15, 17.5, 20, 25, 37.5, 50, or 100%) changed every 60 sec at random order, except that each session was always started with 100% pattern contrast to facilitate acclimatization to the task. Each mouse was tested in at least four trials. The performances across the trials were averaged for analysis, excluding those 60-sec stimulus periods that led to a correct/incorrect ratio smaller than 0.8.

Retinoid analysis—Following completion of ERG and OMR experiments, mice were placed in darkness for 24 hr and then sacrificed. Eyes were excised under dim red light, placed in Eppendorf tubes, flash frozen in liquid nitrogen, and stored at −80 °C. Retinoids were extracted from the whole eyes and analyzed by high-performance liquid chromatography (HPLC) as described previously[44]. 9-*cis*- retinal oxime standard was generated by reacting 9-*cis*-retinal in 50% methanol with excess hydroxylamine, pH 8, and then extracting the resulting 9-*cis*-retinal oximes with hexanes[2]. The retinoid concentration was determined spectrophotometrically using an extinction coefficient (absorptivity *A*352 nm) of 54,119 cm^{-1} M^{-1}. Known amounts of 9-*cis*-retinal oxime were injected onto the HPLC column to allow generation of a standard curve relating *syn*-9-*cis*-retinal oxime mass to elution peak area under the curve. All procedures were performed under dim red light.

Immunohistochemistry—Following euthanasia, mouse eyes were enucleated and fixed for 30 min in PBS containing 4% (w/v) paraformaldehyde (Electron Microscopy Sciences) at room temperature. After fixation, the eyes were incubated at room temperature

sequentially in PBS containing 10%, 20%, and 30% (w/v) sucrose (MilliporeSigma) for 30 minutes at each concentration. Then, the eyes were incubated for 30 minutes at room temperature with a 4:1 mixture of PBS containing 30% sucrose and O.C.T. compound (Fisher Scientific). The eyes were then incubated overnight at 4 °C with a 2:1 mixture of PBS containing 30% sucrose and O.C.T. compound and frozen by immersion in dry ice the next day. Retinal sections were cut at a thickness of 10 μm at −20 °C using a Leica CM1850 cryostat and stored at −80 °C until use. The retinal sections were rehydrated with PBS and then blocked and permeabilized for 30 minutes with 0.2% (v/v) Triton X-100 (Millipore Sigma) and 5% normal goat serum (Abcam) in PBS. The sections were then incubated overnight with anti-Opsin 1, Medium Wavelength primary antibody (1:250; Novus, NB110–74730) in a solution containing 0.2% Triton X-100 and 5% normal goat serum in PBS. The sections were then washed with PBS 3 times, and then incubated with Alexa Fluor 594-conjugated goat anti-rabbit IgG (1:250; Thermo Fisher Scientific, A11037) in PBS. The sections were then washed with PBS 5 times and mounted with VECTASHIELD Mounting Medium containing DAPI (Vector Laboratories) for imaging. Fluorescence images were acquired with a Keyence BZ-X800 All-in-One fluorescence microscope.

QUANTIFICATION AND STATISTICAL ANALYSIS

For ISOI, two-photon calcium and pupil imaging experiments, statistical analyses and data plotting were performed using custom software in R. For all other experiments, statistical analysis was carried out using GraphPad Prism version 9.0. When comparing groups, Shapiro-Wilk normality test was used to test for normality of data. For non-normal data, non-parametric tests such as the Wilcoxon rank sum test were used. In addition to conventional statistical tests, multilevel statistics were employed to take the hierarchical nature of our data into account (*e.g.*, neurons nested inside recording fields, fields nested inside mice). Multilevel linear mixed-effects models with Satterthwaite's approximation were used, with experimental variables (*e.g.*, treatment) as fixed variables and mouse ID and/or field ID as random variables. For each analysis, the exact statistical tests used are described in the figure legends. A P value < 0.05 was considered significant.

Supplementary Material

Refer to Web version on PubMed Central for supplementary material.

Acknowledgments

KP is Donald Bren Professor and Irving H. Leopold Chair of Ophthalmology. Funding was provided by National Institutes of Health grants EY029490 (SPG), EY009339 (KP), EY027283 (KP), EY024864 (KP), the Department of Veterans Affairs I01BX004939 (PDK), and an Unrestricted Grant from Research to Prevent Blindness to Dept. of Ophthalmology, UCI (PDK, KP).

References

1. Chen HY, Lehmann OJ, and Swaroop A. (2021). Genetics and therapy for pediatric eye diseases. EBioMedicine 67, 103360.
2. Acland GM, Aguirre GD, Ray J, Zhang Q, Aleman TS, Cideciyan AV, Pearce-Kelling SE, Anand V, Zeng Y, Maguire AM, et al. (2001). Gene therapy restores vision in a canine model of childhood blindness. Nat. Genet 2001 281 28, 92–95.

3. Suh S, Choi EH, Leinonen H, Foik AT, Newby GA, Yeh W-H, Dong Z, Kiser PD, Lyon DC, Liu DR, et al. (2020). Restoration of visual function in adult mice with an inherited retinal disease via adenine base editing. Nat. Biomed. Eng 2020 52 5, 169–178.

4. Busskamp V, Duebel J, Balya D, Fradot M, Viney TJ, Siegert S, Groner AC, Cabuy E, Forster V, Seeliger M, et al. (2010). Genetic reactivation of cone photoreceptors restores visual responses in retinitis pigmentosa. Science (80-.). 329, 413–17.

5. Goetz GA, and Palanker DV (2016). Electronic approaches to restoration of sight. Reports Prog. Phys 79, 096701.

6. Pearson RA, Barber AC, Rizzi M, Hippert C, Xue T, West EL, Duran Y, Smith AJ, Chuang JZ, Azam SA, et al. (2012). Restoration of vision after transplantation of photoreceptors. Nature 485, 99–103. [PubMed: 22522934]

7. Chen Y, Chen Y, Jastrzebska B, Golczak M, Gulati S, Tang H, Seibel W, Li X, Jin H, Han Y, et al. (2018). A novel small molecule chaperone of rod opsin and its potential therapy for retinal degeneration. Nat. Commun 2018 91 9, 1–18.

8. Hooser JP Van Aleman TS, He Y-G, Cideciyan AV, Kuksa V, Pittler SJ, Stone EM, Jacobson SG, and Palczewski K. (2000). Rapid restoration of visual pigment and function with oral retinoid in a mouse model of childhood blindness. Proc. Natl. Acad. Sci 97, 8623–8628. [PubMed: 10869443]

9. Van Gelder RN, Chiang MF, Dyer MA, Greenwell TN, Levin LA, Wong RO, and Svendsen CN (2022). Regenerative and restorative medicine for eye disease. Nat. Med 28, 1149–1156. [PubMed: 35715505]

10. Koenekoop RK, Sui R, Sallum J, Born LI, van den Ajlan R, Khan A, Hollander den AI, Cremers FPM, Mendola JD, Bittner AK, et al. (2014). Oral 9-cis retinoid for childhood blindness due to Leber congenital amaurosis caused by RPE65 or LRAT mutations: an open-label phase 1b trial. Lancet 384, 1513–1520. [PubMed: 25030840]

11. Scholl HPN, Moore AT, Koenekoop RK, Wen Y, Fishman GA, van den Born LI, Bittner A, Bowles K, Fletcher EC, Collison FT, et al. (2015). Safety and Proof-of-Concept Study of Oral QLT091001 in Retinitis Pigmentosa Due to Inherited Deficiencies of Retinal Pigment Epithelial 65 Protein (RPE65) or Lecithin:Retinol Acyltransferase (LRAT). PLoS One 10, 1–16.

12. Kenna PF, Humphries MM, Kiang A-S, Brabet P, Guillou L, Ozaki E, Campbell M, Farrar GJ, Koenekoop R, and Humphries P. (2020). Advanced late-onset retinitis pigmentosa with dominant-acting D477G RPE65 mutation is responsive to oral synthetic retinoid therapy. BMJ Open Ophthalmol. 5.

13. Gearhart PM, Gearhart C, Thompson DA, and Petersen-Jones SM (2010). Improvement of Visual Performance With Intravitreal Administration of 9-cis-Retinal in Rpe65-Mutant Dogs. Arch. Ophthalmol 128, 1442–1448. [PubMed: 20837787]

14. Ashtari M, Cyckowski LL, Monroe JF, Marshall KA, Chung DC, Auricchio A, Simonelli F, Leroy BP, Maguire AM, Shindler KS, et al. (2011). The human visual cortex responds to gene therapy–mediated recovery of retinal function. J. Clin. Invest 121, 2160–2168. [PubMed: 21606598]

15. Bennett J, Wellman J, Marshall KA, McCague S, Ashtari M, DiStefano-Pappas J, Elci OU, Chung DC, Sun J, Wright JF, et al. (2016). Safety and durability of effect of contralateral-eye administration of AAV2 gene therapy in patients with childhood-onset blindness caused by RPE65 mutations: a follow-on phase 1 trial. Lancet 388, 661–672. [PubMed: 27375040]

16. Aguirre GK, Komáromy AM, Cideciyan AV, Brainard DH, Aleman TS, Roman AJ, Avants BB, Gee JC, Korczykowski M, Hauswirth WW, et al. (2007). Canine and Human Visual Cortex Intact and Responsive Despite Early Retinal Blindness from RPE65 Mutation. PLOS Med. 4, 1–12.

17. Ashtari M, Nikonova ES, Marshall KA, Young GJ, Aravand P, Pan W, Ying G, Willett AE, Mahmoudian M, Maguire AM, et al. (2017). The Role of the Human Visual Cortex in Assessment of the Long-Term Durability of Retinal Gene Therapy in Follow-on RPE65 Clinical Trial Patients. Ophthalmology 124, 873–883. [PubMed: 28237426]

18. Röder B, and Kekunnaya R. (2021). Visual experience dependent plasticity in humans. Curr. Opin. Neurobiol 67, 155–162. [PubMed: 33340877]

19. Foik AT, Lean GA, Scholl LR, McLelland BT, Mathur A, Aramant RB, Seiler MJ, and Lyon DC (2018). Detailed Visual Cortical Responses Generated by Retinal Sheet Transplants in Rats with Severe Retinal Degeneration. J. Neurosci 38, 10709 LP – 10724.

20. Wiesel T, and Hubel D. (1963). Single-cell responses in striate cortex of kittens deprived of vision in one eye. J. Neurophysiol 26, 1003–1017. [PubMed: 14084161]
21. Bavelier D, Levi DM, Li RW, Dan Y, and Hensch TK (2010). Removing brakes on adult brain plasticity: from molecular to behavioral interventions. J. Neurosci 30, 14964–71.
22. Batten ML, Imanishi Y, Maeda T, Tu DC, Moise AR, Bronson D, Possin D, Gelder RN Van Baehr W, and Palczewski K. (2004). Lecithin-retinol Acyltransferase Is Essential for Accumulation of All-trans-Retinyl Esters in the Eye and in the Liver. J. Biol. Chem 279, 10422–10432.
23. Fan J, Rohrer B, Frederick JM, Baehr W, and Crouch RK (2008). Rpe65−/− and Lrat−/− Mice: Comparable Models of Leber Congenital Amaurosis. Invest. Ophthalmol. Vis. Sci 49, 2384–2389. [PubMed: 18296659]
24. Zhang T, Enemchukwu NO, Jones A, Wang S, Dennis E, Watt CB, Pugh EN Jr, and Fu Y. (2015). Genetic deletion of S-opsin prevents rapid cone degeneration in a mouse model of Leber congenital amaurosis. Hum. Mol. Genet 24, 1755–1763. [PubMed: 25416279]
25. Batten ML, Imanishi Y, Tu DC, Doan T, Zhu L, Pang J, Glushakova L, Moise AR, Baehr W, Gelder Van RN, et al. (2005). Pharmacological and rAAV Gene Therapy Rescue of Visual Functions in a Blind Mouse Model of Leber Congenital Amaurosis. PLOS Med. 2, e333. [PubMed: 16250670]
26. Tan L, Tring E, Ringach DL, Zipursky SL, and Trachtenberg JT (2020). Vision Changes the Cellular Composition of Binocular Circuitry during the Critical Period. Neuron 108, 735–747.e6.
27. Larsen RS, and Waters J. (2018). Neuromodulatory correlates of pupil dilation. Front. Neural Circuits 12, 21. [PubMed: 29593504]
28. Kircher N, Crippa SV, Martin C, Kawasaki A, and Kostic C. (2019). Maturation of the pupil light reflex occurs until adulthood in mice. Front. Neurol 10, 56. [PubMed: 30778330]
29. Reimer J, McGinley MJ, Liu Y, Rodenkirch C, Wang Q, McCormick DA, and Tolias AS (2016). Pupil fluctuations track rapid changes in adrenergic and cholinergic activity in cortex. Nat. Commun 2016 71 7, 1–7.
30. Huang S, Gu Y, Quinlan EM, and Kirkwood A. (2010). A Refractory Period for Rejuvenating GABAergic Synaptic Transmission and Ocular Dominance Plasticity with Dark Exposure. J. Neurosci 30, 16636 LP – 16642.
31. Huh CYL, Abdelaal K, Salinas KJ, Gu D, Zeitoun J, Figueroa Velez DX, Peach JP, Fowlkes CC, and Gandhi SP (2020). Long-term monocular deprivation during juvenile critical period disrupts binocular integration in mouse visual thalamus. J. Neurosci 40.
32. Bainbridge JWB, Smith AJ, Barker SS, Robbie S, Henderson R, Balaggan K, Viswanathan A, Holder GE, Stockman A, Tyler N, et al. (2008). Effect of Gene Therapy on Visual Function in Leber's Congenital Amaurosis. N. Engl. J. Med 358, 2231–2239. [PubMed: 18441371]
33. Simonelli F, Maguire AM, Testa F, Pierce EA, Mingozzi F, Bennicelli JL, Rossi S, Marshall K, Banfi S, Surace EM, et al. (2010). Gene therapy for leber's congenital amaurosis is safe and effective through 1.5 years after vector administration. Mol. Ther 18, 643–650. [PubMed: 19953081]
34. Kiser PD, and Palczewski K. (2016). Retinoids and Retinal Diseases. Annu. Rev. Vis. Sci 2, 197–234. [PubMed: 27917399]
35. Gao S, Kahremany S, Zhang J, Jastrzebska B, Querubin J, Petersen-Jones SM, and Palczewski K. (2018). Retinal-chitosan Conjugates Effectively Deliver Active Chromophores to Retinal Photoreceptor Cells in Blind Mice and Dogs. Mol. Pharmacol 93, 438–452. [PubMed: 29453250]
36. Kalatsky VA, and Stryker MP (2003). New paradigm for optical imaging: temporally encoded maps of intrinsic signal. Neuron 38, 529–545. [PubMed: 12765606]
37. Dubbs A, Guevara J, and Yuste R. (2016). moco: Fast motion correction for calcium imaging. Front. Neuroinform 160, 269–290.
38. Kerlin AM, Andermann ML, Berezovskii VK, and Reid RC (2010). Broadly tuned response properties of diverse inhibitory neuron subtypes in mouse visual cortex. Neuron 67, 858–871. [PubMed: 20826316]
39. Chen T-W, Wardill TJ, Sun Y, Pulver SR, Renninger SL, Baohan A, Schreiter ER, Kerr RA, Orger MB, Jayaraman V, et al. (2013). Ultrasensitive fluorescent proteins for imaging neuronal activity. Nature 499, 295–300. [PubMed: 23868258]

40. Salinas KJ, Figueroa Velez DX, Zeitoun JH, Kim H, and Gandhi SP (2017). Contralateral bias of high spatial frequency tuning and cardinal direction selectivity in mouse visual cortex. J. Neurosci 37, 10125–10138.

41. Salinas KJ, Huh CYL, Zeitoun JH, and Gandhi SP (2021). Functional Differentiation of Mouse Visual Cortical Areas Depends upon Early Binocular Experience. J. Neurosci 41, 1470 LP – 1488. [PubMed: 33376158]

42. Jenks KR, and Shepherd JD (2020). Experience-Dependent Development and Maintenance of Binocular Neurons in the Mouse Visual Cortex. Cell Rep. 30, 1982–1994.e4.

43. Leinonen H, Cheng C, Pitkänen M, Sander CL, Zhang J, Saeid S, Turunen T, Shmara A, Weiss L, Ta L, et al. (2021). A p97/Valosin-Containing Protein Inhibitor Drug CB-5083 Has a Potent but Reversible Off-Target Effect on Phosphodiesterase-6. J. Pharmacol. Exp. Ther 378, 31–41. [PubMed: 33931547]

44. Choi EH, Suh S, Sander CL, Hernandez CJO, Bulman ER, Khadka N, Dong Z, Shi W, Palczewski K, and Kiser PD (2018). Insights into the pathogenesis of dominant retinitis pigmentosa associated with a D477G mutation in RPE65. Hum. Mol. Genet 27, 2225–2243. [PubMed: 29659842]

Highlights

- A synthetic retinoid was administered to an adult mouse model of retinal degeneration
- Retinoid treatment partially restored retinal light sensitivity and optomotor response
- Retinoid restored eye-specific responses in V1 via ipsilateral-eye signal enhancement
- Retinoid treatment restored arousal-mediated V1 modulation

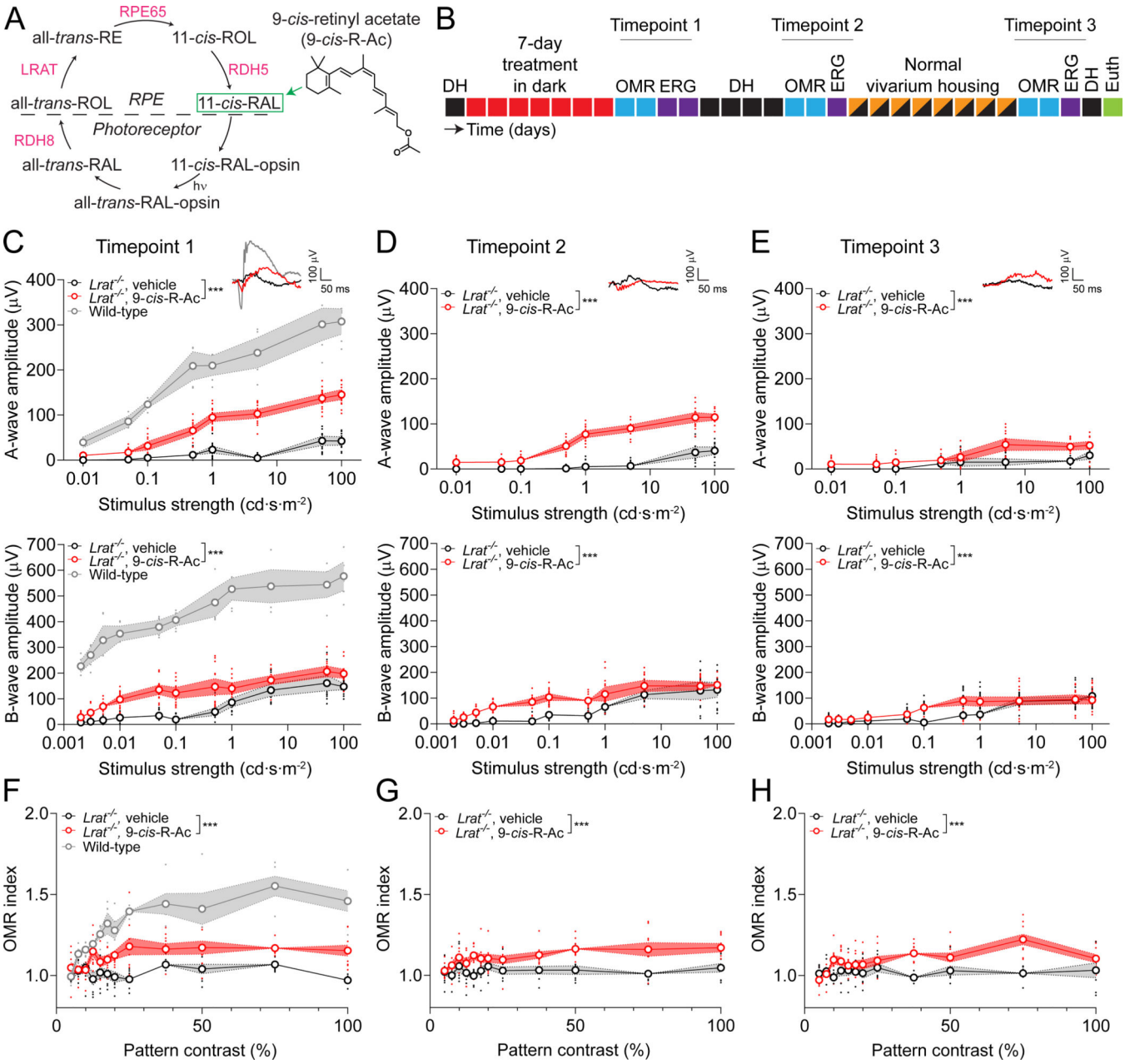

Figure 1. 9-*cis*-retinyl acetate (9-*cis*-R-Ac) partially restored retinal light sensitivity and optomotor response in *Lrat*$^{-/-}$ mice (see also Figures S1, S2).

(**A**) Visual cycle pathway. 9-*cis*-R-Ac was used to replenish the visual chromophore. (**B**) Experimental timeline of drug administration and visual function recording. Each square represents one day. Abbreviations are as follows: DH - dark-housed, OMR – optomotor response, ERG – electroretinography, Euth – euthanized. The treatment consisted of either 40 mg/kg of 9-*cis*-R-Ac in DMSO or DMSO alone (vehicle control) administered *via* intraperitoneal injection. (**C-E**) A-wave (top) and B-wave (bottom) ERG responses obtained at three different timepoints. 9-*cis*-R-Ac-treated mice (n = 18 eyes) showed enhanced ERG responses compared to vehicle-treated mice (n = 14 or 16 eyes; two-way repeated measures ANOVA; *** $P < 0.0001$ with respect to treatment effect). Insets show representative

ERG responses to the 1 cd·s·m-2 flash at each timepoint. (**F-H**) OMR responses. 9-*cis*-R-Ac-treated mice (n = 9 mice) showed significantly enhanced OMR responses compared to vehicle-treated mice (n = 7–8 mice; two-way repeated measures ANOVA; *** $P < 0.0001$ with respect to treatment effect). In panels **C-H**, responses recorded from age-matched wild-type mice (ERG: 8 eyes; OMR: 5 mice) are shown in the left-most panels for comparison. Dots represent individual data points; open circles represent mean values; shaded regions represent 95% CI in **C-E** and SEM in **F-H**.

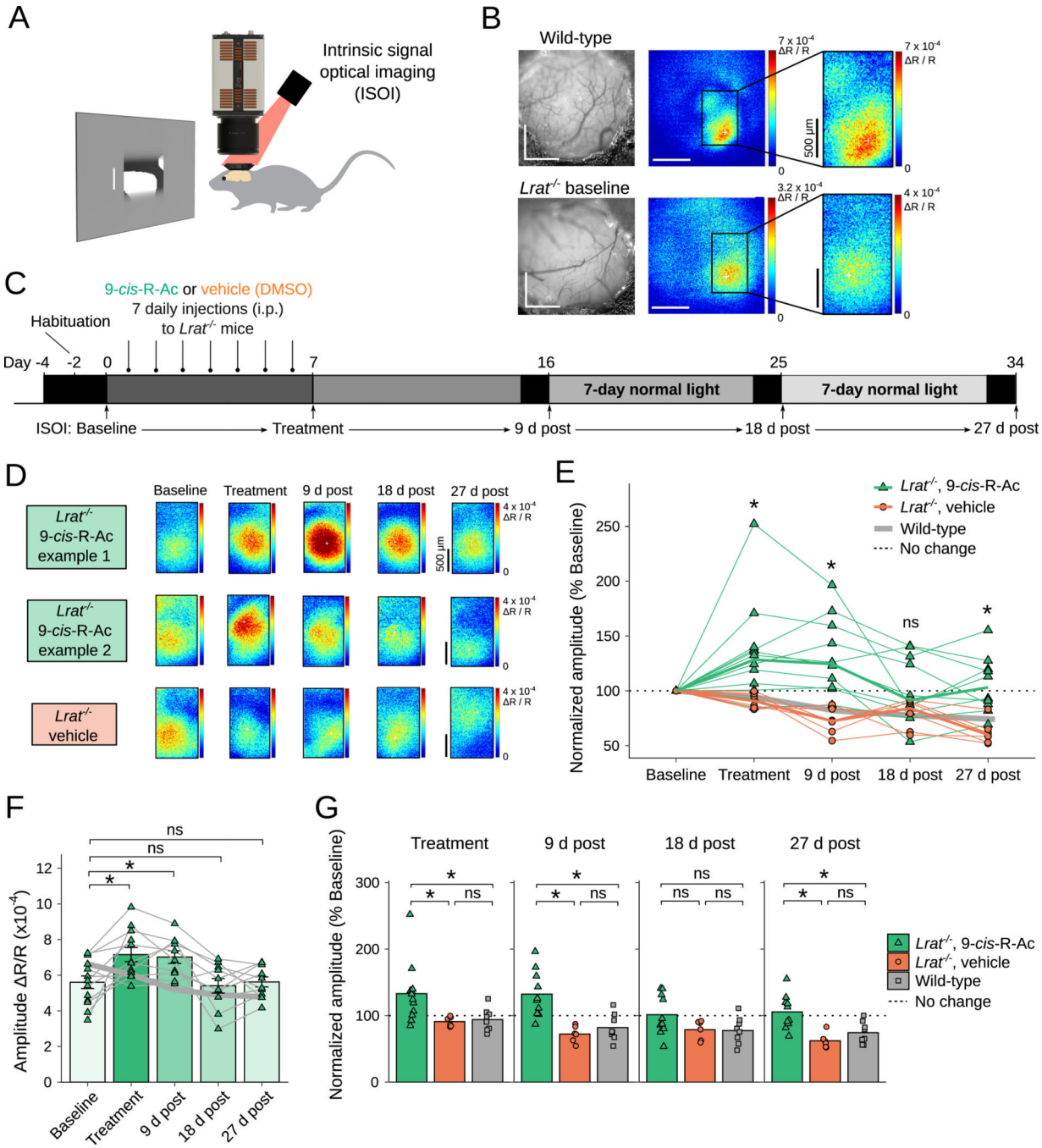

Figure 2. 9-*cis*-R-Ac restored visual responses in V1 of *Lrat*$^{-/-}$ mice (see also Figure S3).

(A) Cortical responses to contrast-reversing central 30° stimuli were recorded using intrinsic signal optical imaging (ISOI). **(B)** The activated area in the binocular zone of visual cortex (V1) is shown in the ISOI amplitude map in example wild-type (top) and *Lrat*$^{-/-}$ mice (bottom). **(C)** Experiment timeline. DH – dark-housed. **(D)** Amplitude maps in retinoid-treated (top two) and vehicle-treated *Lrat*$^{-/-}$ mice (bottom). **(E)** Normalized peak amplitudes. Thin lines: data from the same animal. Thick lines: group medians. Green triangle: 9-*cis*-R-Ac-treated, orange circle: vehicle-treated. Thick gray line: wild-type

median. Dotted line: no change from baseline. Shapiro-Wilk normality test: $P < 0.05$ (data are not normal). Wilcoxon rank sum tests (retinoid- *vs.* vehicle-treated) with BH multiple-comparison correction. **(F)** Peak amplitude values from retinoid-treated *Lrat*$^{-/-}$ mice. Each data point: individual animal. Thick gray line: wild-type mean. Error bars: group mean ± SEM. Shapiro-Wilk normality test: $P > 0.05$ (data are normal). Linear mixed-effects models (baseline *vs.* other timepoints). **(G)** Normalized peak amplitudes. Symbols: individual animals. Green triangle: 9-*cis*-R-Ac-treated *Lrat*$^{-/-}$, orange circle: vehicle-treated *Lrat*$^{-/-}$, gray square: wild-type. Bar plots: group medians. Dotted line: no change from baseline. Shapiro-Wilk normality test: $P < 0.05$. Wilcoxon rank sum tests with BH multiple-comparison correction. $^{*}P < 0.05$, $^{ns}P > 0.05$. n=13 retinoid-treated *Lrat*$^{-/-}$ mice, 6 vehicle-treated *Lrat*$^{-/-}$ mice, 8 wild-type mice.

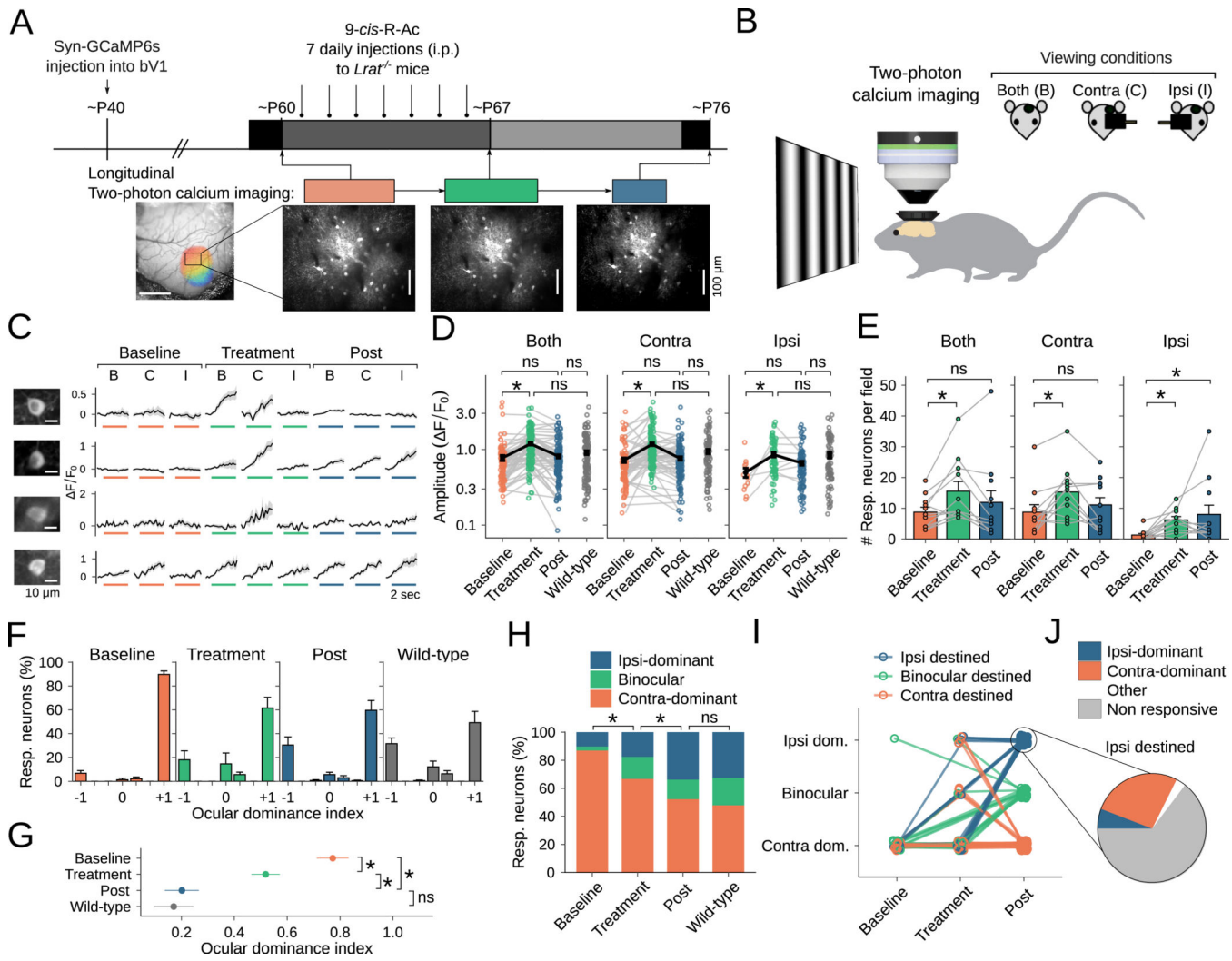

Figure 3. 9-*cis*-R-Ac restored the normal balance of eye-specific responses in V1 of *Lrat*$^{-/-}$ mice (see also Figure S4).

(A) Experiment timeline. Typically the same sets of neurons in the binocular zone of V1 were recorded at baseline, after 9-*cis*-R-Ac treatment and 9 days post treatment. DH – dark-housed. **(B)** Two-photon calcium imaging was performed under three viewing conditions. **(C)** Example calcium traces show responses of four neurons to the same visual stimuli at different timepoints. Black: mean of 8 repeats, gray: mean ± SEM. Bar: stimulus duration. B/C/I: both-eye, contra-eye, ipsi-eye viewing. Left: summed intensity image of neurons whose responses are shown to the right. **(D)** Mean response amplitude of neurons at different timepoints, grouped according to viewing condition. Thin lines: data from the same cells. Thick lines: group mean ± SEM. Amplitudes are log transformed and tested for normality. Shapiro-Wilk normality test: $P > 0.05$ (data are normal). Linear mixed-effects models on log-transformed values (baseline *vs.* other timepoints, treatment and post *vs.* wild-type). **(E)** Number of visually responsive neurons per recording field, grouped according to viewing condition. Thin lines: data from the same fields of view. Error bars: mean + SEM. Shapiro-Wilk normality test: $P < 0.05$ (data are not normal). Wilcoxon rank sum tests (baseline *vs.* other timepoints) with BH multiple-comparison correction. **(F)** Ocular

dominance index distribution shows the balance of eye-specific responses from V1 neurons. Error bars: mean + SEM of fields. **(G)** Mean ocular dominance index. Error bars: mean ± SEM of cells. Shapiro-Wilk normality test: $P < 0.05$. Wilcoxon rank sum tests (baseline *vs.* other timepoints, treatment *vs.* post, post *vs.* wild-type) with BH multiple-comparison correction. **(H)** Ocular dominance distribution of V1 neurons by category. Chi-squared tests with Bonferroni multiple-comparison correction. **(I)** OD identity of V1 neurons at different timepoints, color-coded according to OD destiny (OD identity at post). **(J)** Previous OD identity of V1 neurons with ipsi destiny (total of 68 ipsi-destined cells). Non responsive: not visually responsive prior to post. Other: visually responsive but changed OD identity between baseline and treatment. $^{*}P < 0.05$, $^{ns}P > 0.05$. n=96 visually responsive neurons in 6 *Lrat*$^{-/-}$ mice at baseline, 171 neurons at treatment, 143 at post during both-eye viewing (11–12 fields of view); 120 neurons in 2 wild-type (untreated) mice during both-eye viewing (3 fields of view).

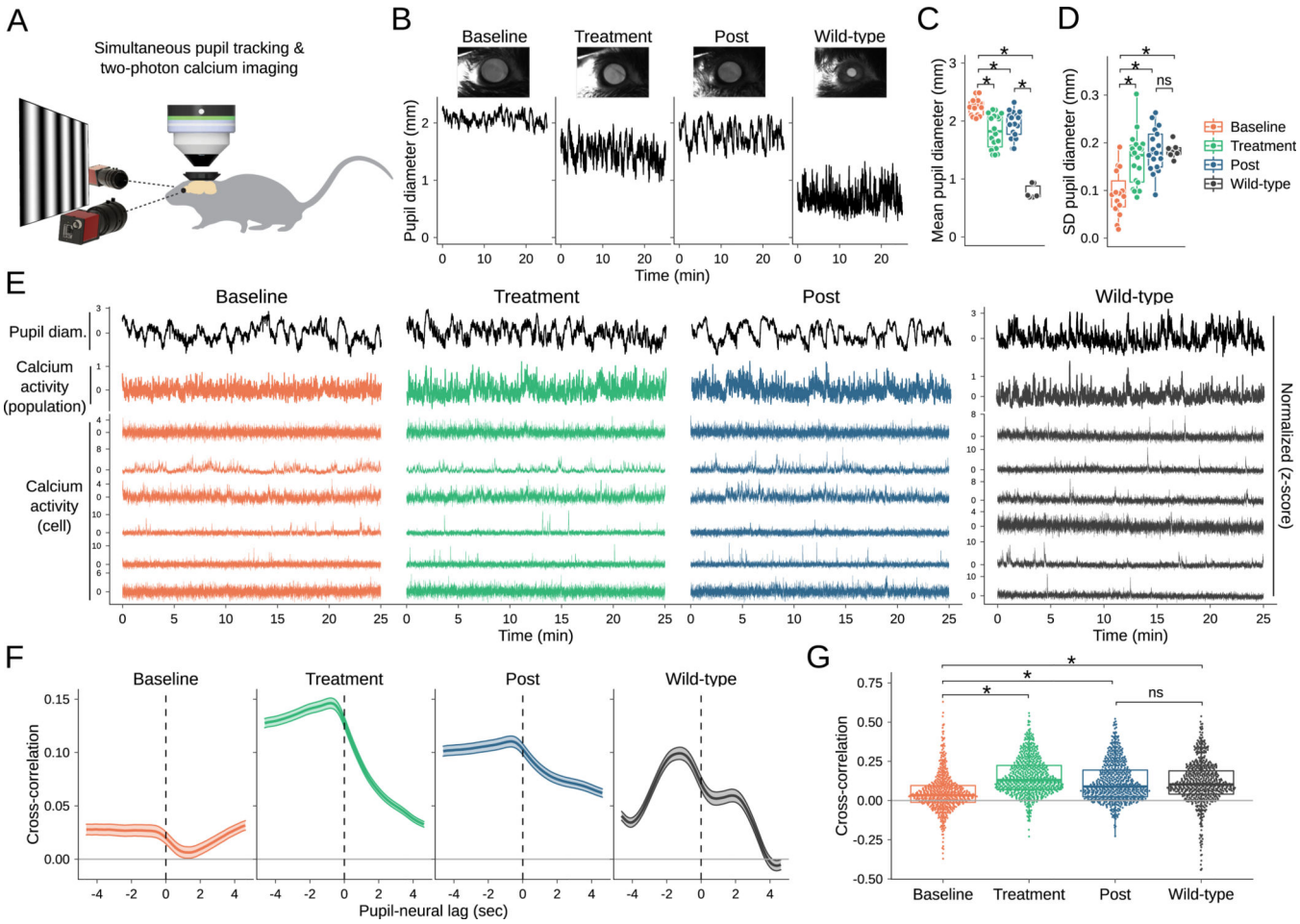

Figure 4. 9-*cis*-R-Ac restored arousal-mediated V1 modulation in *Lrat*$^{-/-}$ mice.

(A) Simultaneous eye recordings and two-photon calcium imaging of V1 neurons. **(B)** Eye images (top) and pupil diameter traces (bottom) from an *Lrat*$^{-/-}$ mouse at baseline, after 9-*cis*-R-Ac treatment and 9 days post treatment, and from an untreated wild-type mouse. **(C,D)** Pupil diameter mean and standard deviation (SD) in 18 recordings in 6 *Lrat*$^{-/-}$ mice and 6 recordings in 2 control mice. Each data point is a recording. Shapiro-Wilk normality test: $P < 0.05$ (data are not normal). Wilcoxon rank sum tests (baseline *vs.* other timepoint, baseline *vs.* wild-type, post *vs.* wild-type) with BH multiple-comparison correction. **(E)** Pupil (top black traces, same traces as B but in z-scores) and calcium traces from six V1 cells that were recorded simultaneously (bottom 6 traces, in z-scores). The second trace from top is the population calcium trace (average of all detected calcium traces of neurons in the field). The first three panels show pupil traces from the same eye and calcium traces from the same neurons in an *Lrat*$^{-/-}$ mouse at different timepoints. The fourth panel shows pupil and calcium traces from a wild-type mouse. **(F)** Cross-correlation values between pupil and calcium traces are shown at different pupil-neural lag windows (negative: neural leading, positive: pupil leading). Vertical dotted line: 0 lag. Mean ± SEM of cells. **(G)** Maximum cross-correlation value per cell is plotted. Each data point is a cell. Shapiro-Wilk normality test: $P < 0.05$. Wilcoxon rank sum tests (baseline *vs.* other timepoints, baseline and post *vs.* wild-type) with BH multiple-comparison correction. **C,D,G**: In box plots, the middle

mark indicates the median, bottom and top edges indicate the 25th and 75th percentiles, respectively. $*P < 0.05$, $^{ns}P > 0.05$. n=654 cells in 6 $Lrat^{-/-}$ mice (11–12 fields of view), 609 cells in 2 wild-type mice (3 fields of view).

KEY RESOURCES TABLE

REAGENT or RESOURCE	SOURCE	IDENTIFIER
Antibodies		
Anti-Opsin 1, Medium Wavelength antibody	Novus	NB110-74730
Alexa Fluor 594-conjugated goat anti-rabbit IgG	Thermo Fisher Scientific	A11037
Alexa Fluor 594-conjugated goat anti-rabbit IgG	Thermo Fisher Scientific	A11037
Bacterial and Virus Strains		
pAAV.Syn.GCaMP6s.WPRE.SV40(AAV1)	[39]	RRID: Addgene_100843
Chemicals, Peptides, and Recombinant Proteins		
retinyl acetate	Sigma-Aldrich	R3250
9-cis-retinyl acetate	[35]	N/A
Deposited Data		
Data	GitHub	https://github.com/careyhuh/retinoid-therapy
Experimental Models: Organisms/Strains		
Mouse: B6;129S6-*Lrat*^{tm1Kpal}/J	The Jackson Laboratory	RRID: IMSR_JAX:018866
Mouse: C57BL/6NCrl	Charles River Laboratories	RRID: IMSR_CRL:027
Mouse: C57BL/6J	The Jackson Laboratory	RRID: IMSR_JAX:000664
Software and Algorithms		
Python PsychoPy v1.9	Python Software Foundation	https://www.python.org
Matlab R2015a	The MathWorks, Inc	https://www.mathworks.com
GraphPad Prism, v 9.4.1	Dotmatics	https://www.graphpad.com/
R, v 3.6.3	The R Foundation for Statistical Computing	https://www.r-project.org/
Analysis code	GitHub	https://github.com/careyhuh/retinoid-therapy
Analysis code	GitHub	https://github.com/careyhuh/rPacu